Divergence Angle of Ions Beams Emanating from an Immersed Radiofrequency Plasma Source

IEPC-2011-166

Presented at the 32nd International Electric Propulsion Conference,
Wiesbaden • Germany
September 11 – 15, 2011

Adam Shabshelowitz[1] and Alec D. Gallimore[2]
University of Michigan, Ann Arbor, Michigan, 48105, USA

Abstract: A radiofrequency (rf) plasma source developed at the Plasmadynamics and Electric Propulsion Laboratory (PEPL) is used to experimentally study the behavior of rf plasma in a magnetic field. The matching network is mounted directly on the plasma source, and the assembly is placed in a vacuum chamber. A Retarding Potential Analyzer (RPA) measures downstream ion beam potentials of an argon plasma from 39 V to 208 V, and Faraday probe measurements give total beam currents from 5.3 mA to 191 mA. The 95% divergence half-angles of the beam are comparable to those reported by Hall thrusters, but further work in a larger facility is required to demonstrate whether the beam current can be increased.

Nomenclature

A_c	=	probe collection surface area
$\|B_y\|$	=	magnitude of axial magnetic field
e	=	elementary charge
$f(V)$	=	voltage distribution function
I_c	=	measured current
I_{axial}	=	integrated total axial current
I_{beam}	=	integrated total beam current
λ	=	effective divergence angle
M_i	=	ion mass
n_i	=	ion number density
r	=	distance from exit plane of plasma source to probe
θ	=	angle from exit plane of plasma source to center of probe
V_{ret}	=	bias potential of ion retarding grid
Z_i	=	ion charge state

I. Introduction

THE use of radiofrequency (rf) plasma in electric propulsion (EP) systems started to be investigated in the 1960s, but it was not until 1992 that the first flight of a rf ion thruster occured.[1,2] Today, there are a variety of EP concepts that employ rf power at various stages of development.[3-10] Particular attention has been paid to helicon plasma sources, since early studies indicated that they may be an efficient source of cold, dense plasma with no exposed electrodes.[11] Observations of ion beams downstream from helicon plasma sources led researchers to believe that a helicon source itself may be appropriate as a thruster,[12,13] but recently published force measurements do not immediately show that helicons produce thrust efficiently.[7,14] Careful study of the sources of inefficiency and accurate measurements of the rf power deposition are required to determine how a helicon thruster might be

[1] Graduate Student, Aerospace Engineering, shab@umich.edu.
[2] Arthur F. Thurnau Professor, Aerospace Engineering, alec.gallimore@umich.edu.

improved. This paper reports probe measurements of a rf plasma source that is placed inside a vacuum chamber at the Plasmadynamics and Electric Propulsion Laboratory (PEPL) at the University of Michigan. The measurements characterize the voltage and the divergence of ion beams emanating from its exhaust with the intent to develop the diagnostic tools necessary to evaluate the source's efficiency as a thruster.

II. Apparatus

A. Facility

The plasma source was positioned inside of the Junior Test Facility (Junior), which is a 3 m long, 1 m diameter vacuum chamber at PEPL. A Leybold MAG 2000 turbomolecular pump backed by an Edwards E1M275S mechanical pump and Edwards EH500 mechanical booster pump evacuates Junior at 1550 L/s on air to a base pressure of 1.0×10^{-6} Torr. Junior is connected to the Large Vacuum Test Facility (LVTF) by a 60 cm diameter gate valve, through which it may use the LVTF's seven CVI TM-1200 nude cryopumps. The cryopumps have a total combined pumping speed of 500,000 L/s on air, and they are able to keep the background pressure below 5×10^{-6} Torr when the gate valve is open and argon is flowing. Figure 1 shows the layout of the experiment at PEPL.

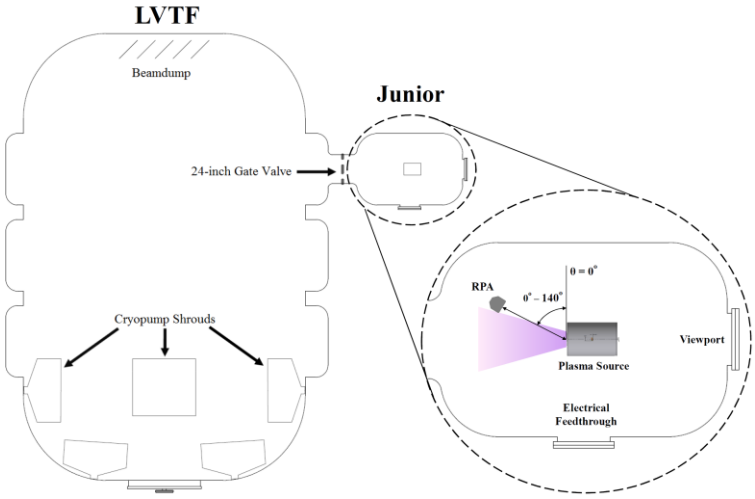

Figure 1. Experiment Layout at PEPL.

B. Plasma Source

The plasma source consists of a quartz tube, an antenna, and six solenoid magnets surrounded by a steel case, and it is represented in Fig. 2(a). The solenoids are capable of producing a uniform axial magnetic field up to 1100 gauss throughout the quartz tube. The steel case enhances both the strength and the uniformity of the magnetic field inside the tube, and prevents a strong magnetic field from persisting outside the source. The antenna is a bifilar, half-turn helical antenna that is intended to excite the m = +1 helicon wave. Multiple layers of flexible mica sheet hold the antenna tightly in the center of the magnet assembly, while insulating it both thermally and electrically from the magnet spools. The quartz tube is 38 cm long with an inner diameter of 9 cm, and it both guides the neutral gas through the magnet assembly and electrically isolates the plasma from the antenna and magnets. The plasma source

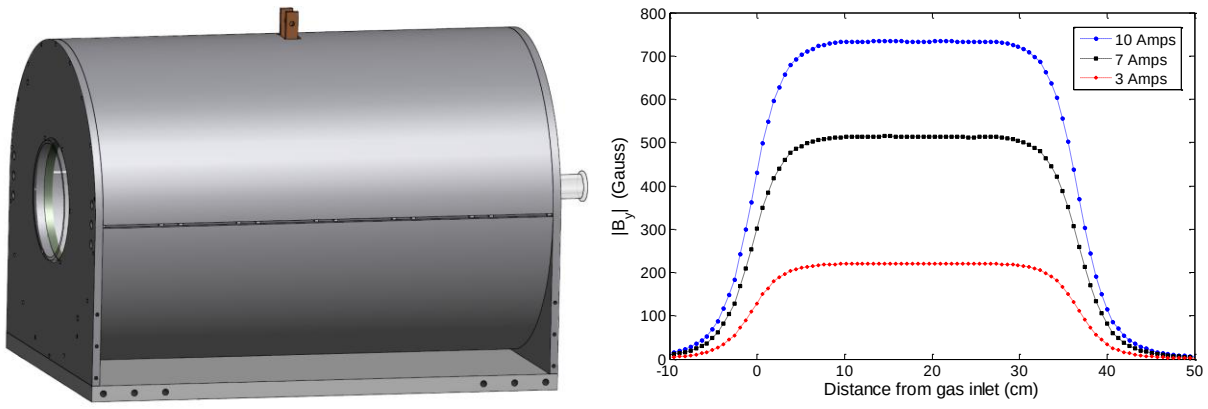

(a) **(b)**

Figure 2. (a) CAD rendering of the assembled plasma source and (b) simulated axial magnetic field strength on centerline for three solenoid currents.

is intended to be operated in vacuum, and was designed to be compatible with the inverted pendulum, null-type thrust stand at PEPL.[15] Simulated magnetic fields are shown in Fig. 2(b). The magnetic field inside the plasma source has been measured at atmospheric pressure with a Lake Shore Cryotronics Model 460 3-channel Gaussmeter in many spatial locations at multiple solenoid currents, and the measured fields were less than 1% different from the simulated fields. Although the antenna is designed to excite the helicon mode, there are no probe measurements taken to determine the coupling mode of the antenna to the plasma, and so it is referred to as the "rf plasma source" or simply the "plasma source" throughout this paper.

C. Rf Power System

A Comdel CPS-3000 rf power supply generates up to 3 kW at a fixed frequency of 13.56 MHz. RG-393 coaxial cables transmit the rf power from the output of the supply first to a Werlatone Model C5389-32 -60dB dual-directional coupler, then through a hermetically-sealed HN-type bulkhead connector at the vacuum chamber feedthrough, and finally to the input of the matching network. The matching network is placed inside of the vacuum chamber in order to reduce the number of impedance discontinuities in the rf power delivery system. Since reflected power increases the uncertainty of the rf power measurements, placing the matching network inside the chamber also increases the confidence that the rf power meters will indicate the actual power being delivered to the load.[16] The forward and reflected voltage waveforms in the cables are continuously monitored using the dual-directional coupler and an oscilloscope, and thermocouples are placed in a few locations on the coaxial cables to ensure that there are no obvious "hot spots", which would be indicative of cable loading when power is reflected.

The matching network is a remotely-controlled pi-L type network with a fixed 1.2 μH inductor, a 20-1000 pF vacuum variable shunt capacitor, and a 12-500 pF vacuum variable tune capacitor. The distance from the matching network output leads to the antenna input leads is made to be as short as possible. A control box that remains outside of the vacuum chamber is used by the operator to turn dc motors that control the capacitor values. Every wire in the control circuitry is passed through rf chokes inside both the matching network and the control box to further discourage the rf power from coupling to the dc components. One side of the matching network is replaced with copper mesh to vent the network of neutral gas, and so that the inside of the matching network can be monitored visually from the viewport on Junior.

D. Probes

A Retarding Potential Analyzer (RPA) and a nude Faraday probe were used in this experiment. Both of these probes have been used to characterize plasma in Hall thruster plumes,[15,17] and the RPA was also used to measure properties in helicon plasmas at PEPL.[18] The probes were placed on two motor stages in the vacuum chamber, one linear and one rotation stage, which allowed the probes to be swept in a constant radius arc centered about the plasma source exhaust. The probes were aligned such that the normal vector through the center of their collection surfaces intersected the center axis of the plasma source at the exit plane of the quartz tube. The RPA floating grid and Faraday probe collection surface remained at a constant distance of 30.5 cm. The angular motion of the probes at this distance is limited by the dimensions of the vacuum chamber, and so the RPA is swept through angles from 0^o to 140^o, as shown in Fig. 1, and the Faraday probe is swept from -10^o to 130^o. The experiment is performed twice, once with the RPA orifice facing the plasma source exit to measure the ion beam potential, and then with the RPA

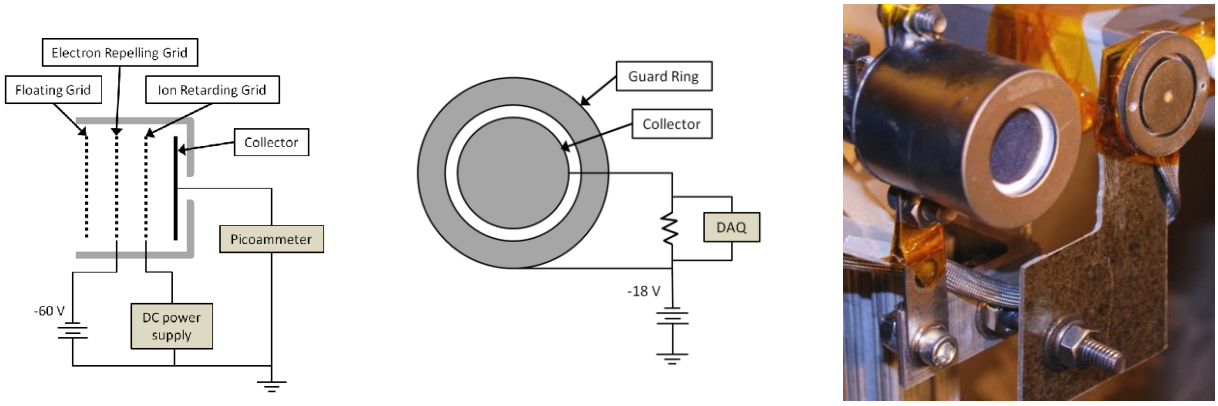

Figure 3. Electrical diagrams for the (a) RPA and (b) Faraday probe, and (c) a picture of the two probes used in this experiment.

turned perpendicular to the flow to measure the bulk plasma potential.[12] Running the experiment twice also demonstrated the repeatability of the Faraday probe measurements. Following the experiment, all data points were repeated with the vacuum chamber at atmospheric pressure to verify that the use of rf alone does not affect the probe measurements.

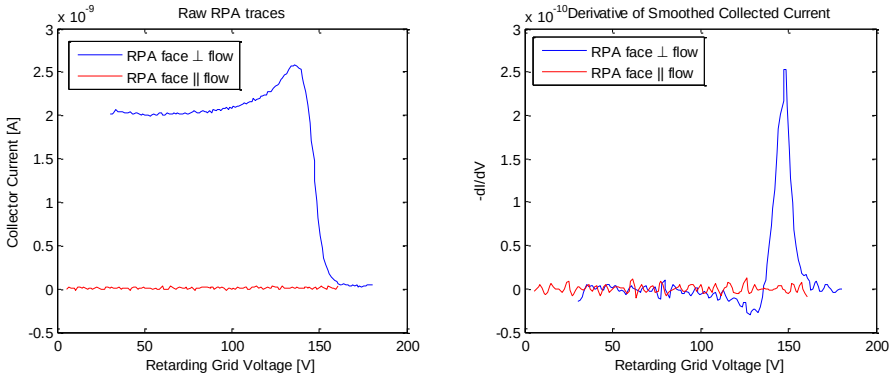

(a) **(b)**

Figure 4. RPA results showing (a) raw I-V characteristics and (b) the first derivative for 10 sccm argon flow rate, 7 A magnet current, and 200 W rf power.

The RPA consists of three grids and a collector contained in a stainless steel case, all isolated from each other and from the case by a macor sleeve and macor spacers. The diagram in Fig. 3(a) shows the arrangement of the grids in the RPA and also represents the electrical schematic. The floating grid first accepts charged particles from the plasma in a minimally disruptive manner. The electron repelling grid is biased to a constant -62 V potential below ground using a high-voltage battery, which prevents the incident electrons from reaching the collector. The bias on the ion retarding grid is swept from 0 V up to 500 V with respect to ground by using a Keithley 2410 SourceMeter to progressively filter out higher potential ions. The current to the collector at each ion retarding voltage is measured using a Keithley 6485 Picoammeter. The first derivative of the current-voltage characteristic is directly proportional to the ion voltage distribution (IVD), as shown in Eq. (1), and so the peak in the first derivative of the I-V characteristic represents the most probable potential of the ion population entering the RPA. Representative results are shown in Fig. 4.

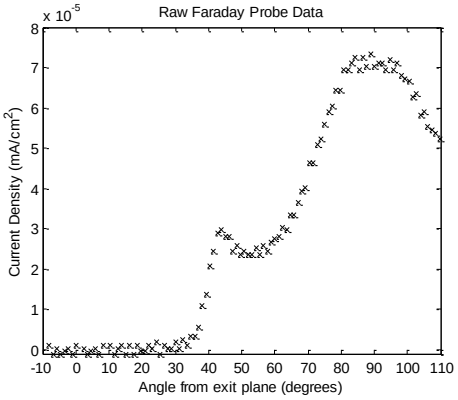

Figure 5. Faraday probe results for 10 sccm argon flow rate, 7 A magnet current, and 200 W rf power. 90° corresponds to plasma source centerline.

Faraday probes are typically employed to measure the current density of the flowing plasma in a thruster plume. The guard ring and the collector are both biased to a potential at which all electrons are repelled, so that the sheath over the collector remains flat. The ion current to the collector is recorded. A diagram of the Faraday probe and electrical circuit is shown in Fig. 3(b). In this experiment, the collection area is taken to be the geometric area of the collector face. The total beam current is calculated from Eq. (2), and the axial component is calculated using Eq. (3) from Faraday probe data taken for 90° of the plume.[19] Representative current density measurements are shown in Fig. 5. The small peak in current density at 40° shown in Fig. 5 is a feature that is present in almost all of the operating conditions analyzed. It appears as either a plateau or a bump at angular locations between approximately 10° and 60°, and may be due to ionization near the walls in the source. The results section further discusses this feature.

$$\frac{dI_c}{dV_{ret}} = -\left(\frac{n_i}{M_i}\right) A_c Z_i^2 e^2 f(V) \tag{1}$$

$$I_{beam} = 2\pi r^2 \int_0^{\pi/2} \frac{I_c(\theta)}{A_c} \sin(\theta) d\theta \tag{2}$$

$$I_{axial} = 2\pi r^2 \int_0^{\pi/2} \frac{I_c(\theta)}{A_c} \cos(\theta)\sin(\theta) d\theta \tag{3}$$

III. Results

Unpublished results from a previous experiment using this plasma source showed that an ion population with a double-peaked IVD was emanating from the source exit, similar to that found in other devices.[12,20] The results of that experiment qualitatively showed that the relative magnitude of the lower voltage IVD peak decreased and the potential of the higher voltage peak increased with decreasing flow rate and with increasing magnetic field. The results of the previous experiment also guided the selection of operating points for this experiment. For almost all of the conditions presented here, there was no population of ions observed when the RPA face was parallel to the flow, as shown in Fig. 4. RPA data were recorded at multiple angular locations, and the normalized IVD did not change significantly with angular location, except at the angles where the current density approached zero, at which the IVD showed no presence of ions. The Faraday probe results are well-represented by Fig. 5, with a side peak or plateau in the current density profile occurring at an angular location between approximately 10^o and 60^o for almost all of the source operating conditions. Qualitatively, the side peak magnitude increases with power, and its angular location moves away from the centerline with increasing magnetic field and with increasing argon flow rate. This side peak may be the result of near-wall ionization increasing the density at the edge of the plasma due to capacitive coupling near the antenna in the quartz tube. If the ions remain at room temperature, the argon gyroradius in a 220 Gauss magnetic field is only 4.7 mm, and so cold ions are magnetized until they reach the exit of the quartz tube at all conditions presented here.

The most probable potential and total current observed are summarized in Fig. 6. For the integrations in Eq. (2) and (3), the plasma source is assumed to be a point source of ions, and the collected current density is integrated from 0^o to 90^o. Note that the magnet current has a much larger effect on the total beam current than power. This may indicate that there is a population of ions with a temperature perpendicular to the magnetic field that is much warmer than room temperature, and that the magnetic field significantly reduces the amount of ions lost to the wall inside the source. Operating conditions at higher flow rates and with stronger magnetic field settings produced a stronger coupling mode that indicated current densities much greater than those in Fig. 6, but also prevented reliable probe operation.

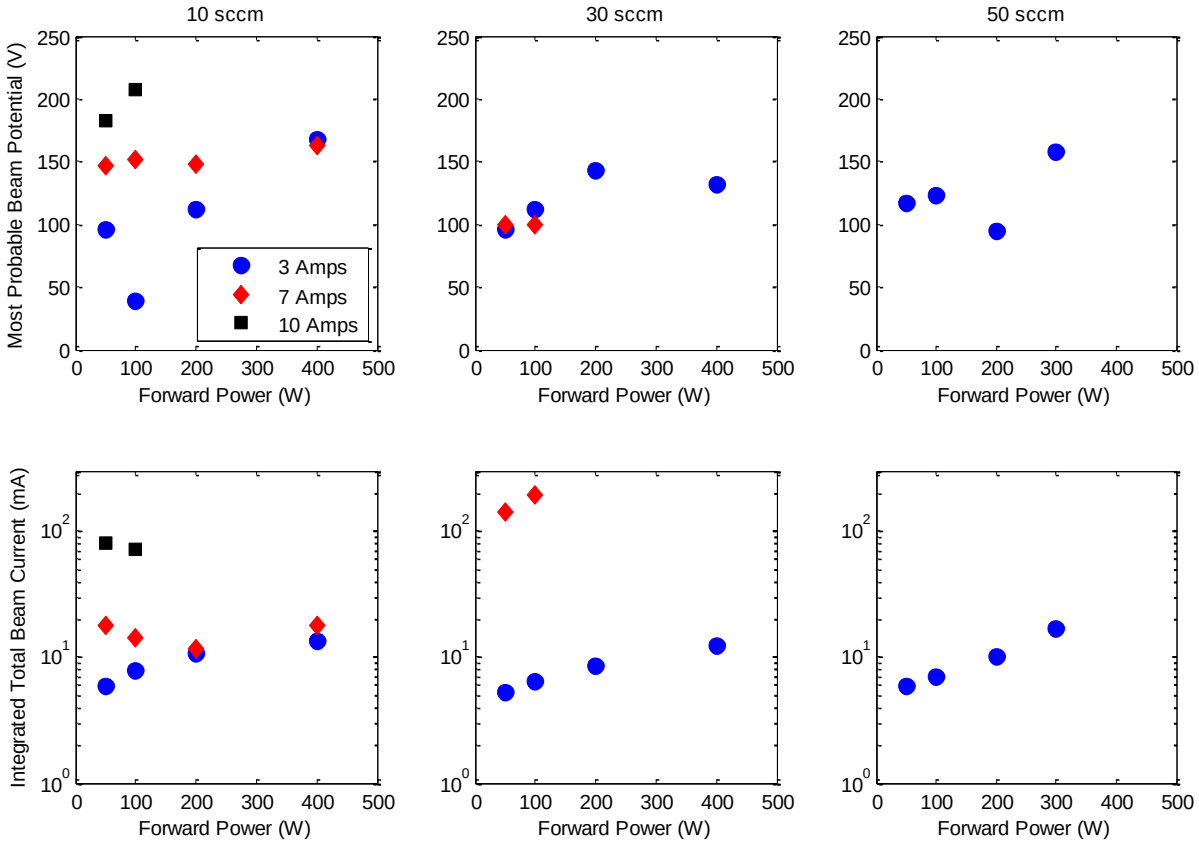

Figure 6. Summary of beam voltage and current results for three argon flow rates. The legend in the first subplot refers to the current through the solenoid magnets, and applies to all plots.

An effective divergence angle is determined using Eq. (4) and the quantities calculated from Eqs. (2) and (3).[21]

$$\lambda = \cos^{-1}\left(\frac{I_{axial}}{I_{beam}}\right) \tag{4}$$

Another method for expressing the divergence of the beam is by integrating the current with Eq. (2) from the centerline outward until 95% of the total current is obtained. The angle at which this occurs is referred to as the "95% divergence half-angle", and it a more accurate quantity for representing cosine losses in a thruster.[21] Both the effective divergence angle and the 95% divergence half-angle are plotted in Fig. 7.

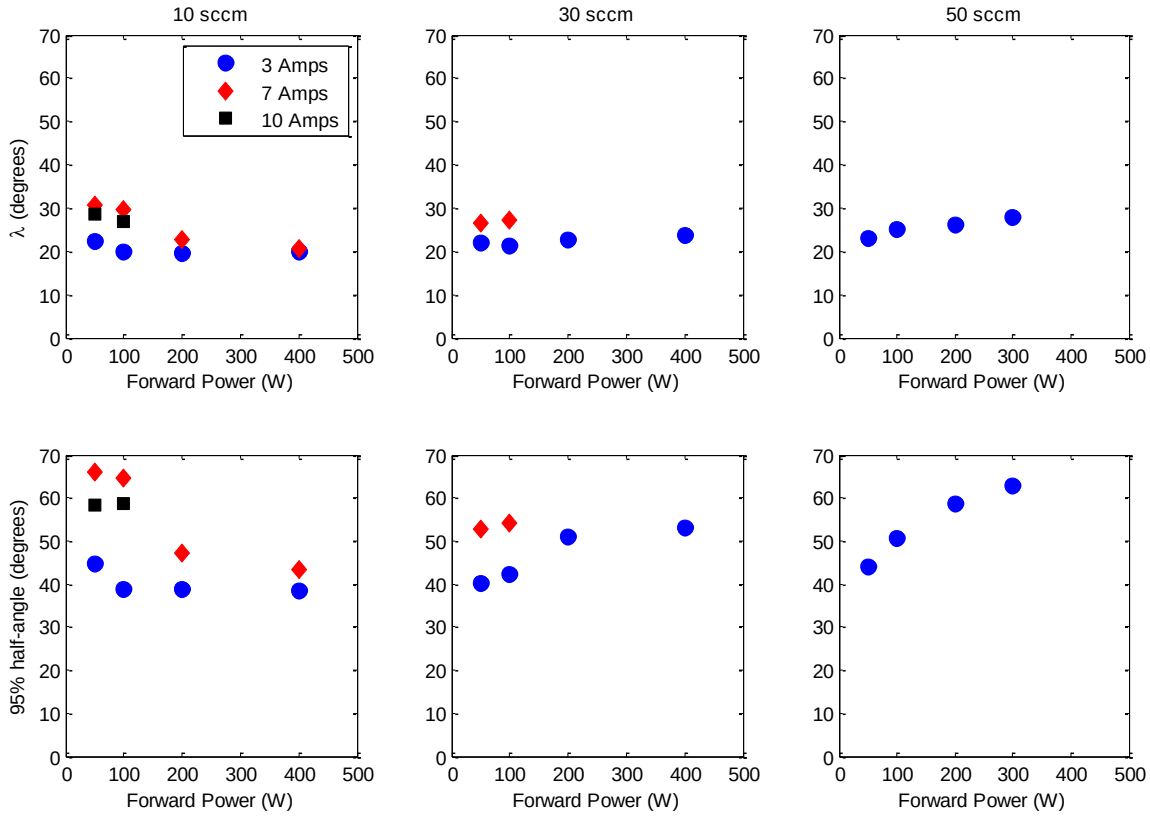

Figure 7. Summary of divergence results for three argon flow rates. The legend in the first subplot refers to the current through the solenoid magnets, and applies to all plots.

The divergence of the plasma downstream of the source tends to increase slightly with increasing flow rate. Both the trend with flow rate and the specific values of divergence angle are similar to those reported in a Hall thruster.[21] The divergence angle increased when increasing magnet current from 3 A to 7 A, but then decreased from 7 A to 10 A, and so the overall trend of divergence with magnetic field is not evident. Rf power has a stronger influence at higher flow rates, where the divergence tends to increase with increasing rf power.

IV. Conclusion

A rf plasma source and its matching network have been operated in the vacuum chamber at PEPL, and probe measurements have characterized the plasma that it produces. The set of data presented in this paper is limited because an increase in any one of the varied parameters (argon flow rate, magnetic field strength, or rf power) produced a coupling mode that dramatically increased the observed brightness of the plasma and the current density measured by the Faraday probe, but was also accompanied by the onset of frequent micro-arcing to the inside wall of the vacuum chamber, which prevented the probes from collecting consistent data. This micro-arcing is attributed to a facility effect that is not anticipated to be present in larger vacuum chambers, such as the LVTF. From Fig. 6, it is clear that low-pressure, low-power operation of this rf plasma source in vacuum produces a population of ions with a high potential that is directed, although with a low total beam current. The current density profiles all contain an interesting side-peak feature that may relate to the coupling mode of the antenna to the plasma. The divergence of

the ion beam emanating from the rf plasma source is comparable to the divergence seen in Hall thruster plumes.[21] The divergence angle increases with flow rate and rf power, but the trend with magnetic field is not monotonic. Further testing in the LVTF is planned to explore higher power operation of the plasma source, which may change the coupling mode and increase the current density of the ion beam.

Acknowledgments

The authors would like to thank Anthony Sebastian at the University of Michigan's Lurie Nanofabrication Facility for his helpful advice on matching, and the National Science Foundation for providing financial support for this research.

References

[1]Goebel, D. M., and Katz. I., *Fundamentals of Electric Propulsion: Ion and Hall Thrusters*, Wiley, New York, 2007, Chap. 9.

[2]Groh, K. H., and Loeb, H. W. "State of the art radio-frequency ion sources for space propulsion," *Review of Scientific Instruments*, Vol. 65, No. 5, May 1994, pp. 1741-1744.

[3]Longmeir, B. W., et al., "VX-200 Magnetoplasma Thruster Performance Results Exceeding Fifty-Percent Thruster Efficiency," *Journal of Propulsion and Power*, Vol. 27, No. 4, July-August 2011, pp. 915-920.

[4]Martinez, R. A., Hoskins, W. A., Peterson, P., and Massey, D., "Development Status of the Helicon Hall Thruster," *31st International Electric Propulsion Conference*, IEPC-2009-120, Ann Arbor, MI 2009.

[5]Kirtley, D., Gallimore, A. D., Haas, J., and Reilly, M., "High Density Magnetized Toroid Formation and Translation within XOCOT: An Annular Field Reversed Configuration Plasma Concept," *30th International Electric Propulsion Conference*, IEPC-2007-04, Florence, Italy, 2007.

[6]Choueiri, E. Y., and Polzin, K. A., "Faraday Acceleration with Radio-Frequency Assisted Discharge," *Journal of Propulsion and Power*, Vol. 22, No. 3, May-June 2006, pp. 611-619.

[7]Pottinger, S., Lappas, V., Charles, C., and Boswell, R., "Performance characterization of a double layer thruster using direct thrust measurements," *Journal of Applied Physics D: Applied Physics*, Vol. 44, No. 23, 15 June 2011.

[8]Motomura, T., et al., "Novel Electromagnetic Propulsion System Using High-Density Helicon Plasma," *52nd Annual Meeting of the APS Division of Plasma Physics*, Chicago, IL, 2011.

[9]Pavarin, D., et al., "Design of 50 W Helicon Plasma Thruster," *31st International Electric Propulsion Conference*, IEPC-2009-205, Ann Arbor, MI, 2009.

[10]Winglee, R, Ziemba, T., Giersch, L., Prager, J., Carscadden, J., and Roberson, B. R., "Simulation and laboratory validation of magnetic nozzle effects for the high power helicon thruster," *Physics of Plasmas*, Vol. 14, No. 6, June 2007.

[11]Chen, F. F., "Plasma ionization by helicon waves," *Plasma Physics and Controlled Fusion*, Vol. 33, No. 4, April 1991, pp. 339-364.

[12]Charles, C., and Boswell, R. W., "Laboratory evidence of a supersonic ion beam generated by a current-free "helicon" double-layer," *Physics of Plasmas*, Vol. 11, No. 4, April 2004, pp. 1706-1714.

[13]Sun, X., et al., "Observations of Ion-Beam Formation in a Current-Free Double Layer," *Physical Review Letters*, Vol. 95, No. 2, July 2005.

[14]Williams, L., and Walker, M. L. R., "Thrust Measurements of a Helicon Plasma Source," *47th AIAA/ASME/SAE/ASEE Joint Propulsion Conference & Exhibit*, San Diego, CA, 2011.

[15]Hofer, R. R., "Development and Characterization of High-Efficiency, High-Specific Impulse Xenon Hall Thrusters," Ph.D. Dissertation, Department of Aerospace Engineering, University of Michigan, Ann Arbor, MI, 2004.

[16]Garvin, C., Grimard, D., Grizzle, J., and Gilchrist, B.E., "Measurement and error evaluation of electrical parameters at plasma relevant frequencies and impedances," *Journal of Vacuum Science & Technology A*, Vol. 16, No. 2, March-April 1998, pp. 595-606.

[17] Walker, M. L. R., Hofer, R. R., and Gallimore, A. D., "The Effects of Nude Faraday Probe Design and Vacuum Facility Backpressure on the Measured Ion Current Density Profile of Hall Thruster Plumes," *38th AIAA/ASME/SAE/ASEE Joint Propulsion Conference & Exhibit*, AIAA-2002-4253, Indianapolis, IN, 2002.

[18]Lemmer, K. M., "Use of a Helicon Source for Development of a Re-Entry Blackout Amelioration System," Ph.D. Dissertation, Department of Aerospace Engineering, University of Michigan, Ann Arbor, MI, 2009.

[19]Wiebold, M., Sung, Y., and Scharer, J. E., "Experimental observation of ion beams in the Madison Helicon eXperiment," *Physics of Plasmas*, Vol. 8, No. 6, June 2011.

[20]Brown, D. L., "Investigation of Low Discharge Voltage Hall Thruster Characteristics and Evaluation of Loss Mechanisms," Ph. D. Dissertation, Department of Aerospace Engineering, University of Michigan, Ann Arbor, MI, 2009.

[21]Brown, D. L., Larson, C. W., Beal, B. E., and Gallimore, A. D., "Methodology and Historical Perspective of a Hall Thruster Efficiency Analysis," *Journal of Propulsion and Power*, Vol. 25, No. 6, November-December 2009, pp. 1163-1177.